PHYSICAL REVIEW A VOLUME 42, NUMBER 5 1 SEPTEMBER 1990

Switching dynamics of finite periodic nonlinear media: A numerical study

C. Martijn de Sterke and J. E. Sipe
Department of Physics, University of Toronto, Toronto, Ontario, Canada M5S 1A7
and Ontario Laser and Lightwave Research Centre, University of Toronto, Toronto, Ontario, Canada M5S 1A7
(Received 26 March 1990)

Using a coupled-mode approach we numerically investigate the time-dependent properties of nonlinear periodic media of finite length. Based on time-independent considerations such media have been shown previously to exhibit bistable behavior and to support gap soliton excitations. Our calculations show that for low intensities the transition from a low-transmission to a high-transmission state occurs as expected, leading to an easy excitation of gap solitons. At higher intensities, however, periodic self-oscillations take place, which eventually turn chaotic.

I. INTRODUCTION

Gap solitons were first observed a few years ago by Chen and Mills in numerical simulations of optical nonlinear periodic media.[1] Their work showed that radiation with a frequency falling within the stop gap of such structures can, for certain values of the intensity, be perfectly transmitted; recall that a linear periodic structure strongly reflects such radiation. Chen and Mills conjectured that this behavior was due to the excitation of a resonance—a "gap soliton"—in the nonlinear periodic medium, a view that was subsequently confirmed by de Sterke and Sipe in a theoretical study.[2] Continued interest in gap solitons and related phenomena is driven by both practical as well as fundamental considerations. Examples of the former are possibilities for bistability and low-energy switching,[3] for low-velocity energy transport,[4] and for modal-dispersion cancellation in fibers.[5] More fundamental interests focus on the nonlinear dynamics of gap solitons,[6,7] and on the possibility for the existence of higher-order solitary-wave solutions.

The physical mechanism behind the properties of gap solitons in nonlinear periodic media can be easily explained. The incoming radiation is chosen to have a frequency falling within one of the stop gaps, but through the nonlinearity the electric field may shift the photonic band structure such that the center frequency corresponds to an allowed band. Locally, therefore, the system now allows traveling-wave solutions, which, as discussed in detail previously,[2] can lead to the perfectly transmitting state of the medium. Obviously, when the center frequency is close to one of the edges of the gap and the nonlinearity has the appropriate sign, the necessary field strength to accomplish this is minimized. The low-intensity limit can thus be obtained by tuning close to the appropriate edge of the stop gap.

The reported research in this area has thus far been of a theoretical nature only. These efforts can be roughly divided into four categories. In the first of these, one makes use of a nonlinear analog of the techniques used in the design of linear thin-film stacks. These methods, which give exact[1,3] or approximate[8] time-independent solutions to the full nonlinear wave equation, have the disadvantage that it can be hard to extract general information from the numerical results. For example, in numerical experiments one can only indirectly demonstrate if a gap soliton has been excited.[1,8] In the second approach one replaces the periodic nonlinear medium by a model structure in which the nonlinear dielectric is assumed to be concentrated on equidistant δ-function-like sheets surrounded by vacuum.[7,9] This rather artificial model has the advantage that the dynamics is described by difference equations rather than differential equations, thus considerably reducing the computational requirements. It demonstrates numerically the possibility for the propagation and interaction of solitonlike objects. The problem with this approach is that it is not clear *a priori* which features are genuine and which are artifacts of the model. For example, this model has the property that positive and negative nonlinearities lead to qualitatively different behavior,[9] in contrast to the nature of continuous systems as found by both analytic and numerical analyses. The third class of methods is based on techniques from solid-state physics. In this method one writes the electric field as the product of a suitably chosen Bloch function of the linear structure and a slowly varying envelope.[2,4,10] This envelope function has been shown to satisfy the nonlinear Schrödinger equation.[2] The separation between the rapidly varying Bloch function and the slowly varying envelope is an important advantage of this method: It is the envelope function that is physically most important, and it can be studied in isolation using the nonlinear Schrödinger equation with appropriate boundary conditions.[2] It should be noted that this method gives solutions to the full wave equation in the low-intensity limit, which, as mentioned above, can be selected by tuning the incoming radiation close to the edge of the stop gap. The fourth class of methods is based upon a set of coupled-mode equations, rather than on the wave equation itself, and attempts to find exact solutions to these equations.[5,6,11,12] Using this approach, one is not restricted to solutions at the edge of the stop gap, thus allowing solutions at any level of intensity. The coupled-mode equations, however, treat the periodicity to first order only,[5,6,11,12] and can thus only be used for structures with a small modulation depth. However, this

is often a good approximation in geometries like optical waveguides and fibers, which typically have modulation depths of only about 10^{-3} and 10^{-6}, respectively. Thus far the work based on the coupled-mode equations has been restricted to systems of infinite extent only. It has made use of a similarity between the coupled-mode equations and those of the Thirring model from field theory, of which the latter are known to be integrable.[13] In this way it has been shown that the coupled-mode equations allow solitary-wave solutions, which, at least on an infinite interval, appear to be stable.[6] The coupled-mode approach shares the advantage of the third class of methods in that one only deals with envelope functions[5,6,14] rather than with the electric field itself, thus again substantially facilitating the analysis. In the coupled-mode approach, however, the envelope functions modulate the forward- and backward-traveling waves, rather than Bloch functions.[2,10]

In the present paper we extend the analysis based upon the coupled-mode equations by investigating its solutions on a finite interval using numerical techniques. We use the coupled-mode approach because of its ability to describe the system's response at both high- and low-intensity levels, while avoiding the difficulties involved in solving the full wave equation. In the low-intensity limit we find agreement with our previous work[2] based upon the nonlinear Schrödinger equation. This regime, in which gap solitons can easily be excited, is characteristic of integrable systems. However, at higher field strengths we find solutions with a chaotic behavior, a property commonly associated with nonintegrable systems. This chaotic behavior is related to a strange attractor that is characterized by a fractal dimension and by a positive Lyapunov exponent. This demonstrates the extremely varied dynamics of finite systems, a richness that would have to be understood before considering any potential application. The emphasis in the present paper, however, is on the numerical results. A detailed analysis of dynamics has proven to be very involved and is still in progress. We therefore discuss our results on a qualitative level here, deferring an in-depth analysis to a future publication.

Our investigations follow earlier work by Winful and Cooperman.[14] These authors consider a similar problem, but with a slightly more complicated optical nonlinearity. However, they investigate a very small part of the available phase space and only find solutions in the high-intensity limit, thus completely missing the regime in which the soliton properties dominate. A very important difference is that Winful and Cooperman switch on the driving fields instantaneously, whereas we do so gradually, thus ensuring information on the system's differential response. In this way we can also best compare our results with the well-known time-independent solutions.

This paper is structured as follows. In Sec. II we discuss the coupled-mode equations and their time-independent solutions. In Sec. III we first briefly describe our integration procedure and then we give a detailed presentation of our numerical results. In Sec. IV, finally, we discuss these results qualitatively, identifying some of the probable elements of a more comprehensive analysis.

II. COUPLED-MODE EQUATIONS AND TIME-INDEPENDENT SOLUTIONS

We consider the interaction of a nonlinear, weakly periodic structure and an (almost) Bragg matched optical field which travels in the directions perpendicular to the grating planes. Taking the nonlinearity of the simple Kerr type, we can write the index of refraction as

$$n(x,z)=n_0(x)+n_1(x)\cos(2\pi z/d)+n_2(x)|\mathbf{E}(x,z)|^2 , \tag{1}$$

where $\mathbf{E}$ is the electric-field amplitude. Further, the z coordinate defines the grating direction, whereas x denotes some transverse coordinate(s). Note that the assumption of a Kerr nonlinearity implies an instantaneous, nondiffuse nonlinear response. The use of the coupled-mode formalism now requires that the linear modulation is weak,[15] or

$$n_1 \ll n_0 . \tag{2}$$

It is not necessary to specify our structure in more detail, and the formalism therefore applies to a variety of geometries. These include thin-film stacks, as well as optical waveguides[16] and fibers.[17] For the latter two geometries, however, Eqs. (1) and (2) describe the distribution of an effective, or mode index,[16,17] rather than "the" index of refraction. The use of the coupled-mode formalism requires further that the wave-number distribution of the electric field inside the structure is narrow[18] and peaks around a value k, such that the detuning δ, defined through

$$\delta=k-\pi/d , \tag{3}$$

satisfies[15]

$$\delta \ll \pi/d . \tag{4}$$

Inequality (4) assures that the field and the grating are (almost) phase matched, so that forward- and backward-traveling modes interact strongly through Bragg reflection.

In using the coupled-mode approach one seeks solutions for the electric field as the sum of suitably modulated forward- and backward-traveling modes:

$$\mathbf{E}(x,z,t)=[\mathcal{E}_+(z,t)e^{-i(\omega t-kz)}+\mathcal{E}_-(z,t)e^{-i(\omega t+kz)}] \times \mathbf{f}(x;\omega)+\text{c.c.} , \tag{5}$$

where c.c. denotes complex conjugate, and $\mathcal{E}_\pm$ are envelope functions of the forward- and backward-traveling modes, which are assumed to be slowly varying in space and time. Further, ω is an optical frequency to be discussed below, and $\mathbf{f}$ is a suitably defined mode of the geometry, which reduces to a constant for a thin-film stack. If we now define

$$\mathcal{E}_\pm(z,t)=\mathcal{F}_\pm(z,t)e^{\mp i\delta z} , \tag{6}$$

it can be shown that the envelope functions $\mathcal{F}_\pm$ satisfy the set of coupled-mode equations[5,6,12,14,18]

$$+i\frac{\partial \mathcal{F}_+}{\partial z}+i\frac{\eta}{c}\frac{\partial \mathcal{F}_+}{\partial t}+\delta\mathcal{F}_+ +\kappa\mathcal{F}_- +\Gamma_s|\mathcal{F}_+|^2\mathcal{F}_+ +2\Gamma_\times|\mathcal{F}_-|^2\mathcal{F}_+ =0\ ,$$
$$-i\frac{\partial \mathcal{F}_-}{\partial z}+i\frac{\eta}{c}\frac{\partial \mathcal{F}_-}{\partial t}+\delta\mathcal{F}_- +\kappa\mathcal{F}_+ +\Gamma_s|\mathcal{F}_-|^2\mathcal{F}_- +2\Gamma_\times|\mathcal{F}_+|^2\mathcal{F}_- =0\ , \tag{7}$$

where c/η is the group velocity of the unperturbed modes, and κ is a coupling coefficient which may be extracted from experiments or from a detailed calculation of the interaction between field and grating. The parameters Γ_s and $\Gamma_\times$ are overlap integrals of the field and the nonlinearity, and denote the self- and cross-phase modulation of the modes, respectively. All coefficients in the coupled-mode equations are assumed to be real, implying the absence of linear as well as nonlinear losses. In the present paper we further restrict ourselves to

$$\Gamma_s=\Gamma_\times\equiv\Gamma\ , \tag{8}$$

which is a very good approximation for mode propagation in waveguides and fibers.[17] Note that one could absorb the third terms in Eqs. (7) in the general time dependence of the fields by rewriting the coupled-mode equations in terms of the envelope functions $\mathcal{F}'_\pm=\mathcal{F}_\pm\exp(ic\delta t/\eta)$, but we have found it more convenient to work with Eqs. (7).

To elucidate further the significance of inequality (4) and of the various parameters we refer to Fig. 1, which shows the dispersion relation of the *linear* periodic structure as following from the coupled-mode equations. The dashed lines give the dispersion relations in the limit of a vanishing grating ($\kappa\to 0$), whereas the solid line gives the dispersion relation when the modulation depth attains a finite value. Note that the former are assumed to be straight (with slopes of $\pm c/\eta$), which is not quite true in general. As we saw before, the use of the coupled-mode formalism not only requires the gap to be small, but also the frequency and wave-number content of the field to be concentrated in and around the gap. In the light of this restriction we are only interested in a small part of the total dispersion curves, and in this region the neglect of the curvature is a good approximation in general. We define ω_0 to fall in the middle of the stop gap (Fig. 1), and, since the unperturbed dispersion curves are assumed to be straight, an angular frequency of $\omega=\omega_0+(c/\eta)\delta$, gives rise to a detuning δ. It should be mentioned that if $-\kappa\le\delta\le\kappa$, the radiation falls inside the gap, whereas otherwise it corresponds to an allowed band.

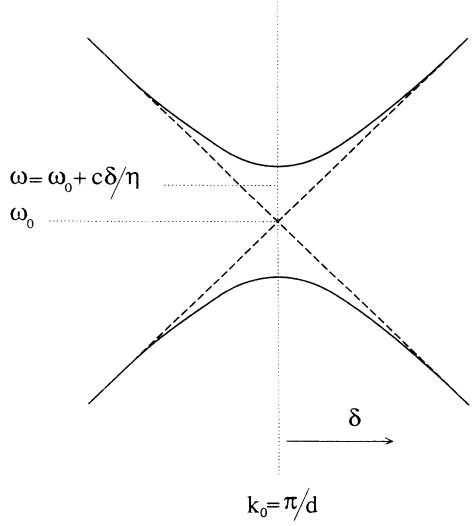

FIG. 1. Dispersion relations following from the coupled-mode equations at the edge of the Brillouin zone. The dashed lines, which have a slope of c/η, show the limit in which the grating vanishes ($\kappa\to 0$), whereas the solid lines refer to a finite grating. The size of the stop gap is $2\kappa c/\eta$.

The system of coupled-mode equations has been shown to have solitary-wave solutions which can propagate at any given speed between zero and c/η.[6] In the present paper we consider solutions to the coupled-mode equations on a *finite* interval of length L, where these solitary waves are no longer solutions. Specifically, we consider a geometry as in Fig. 2, and take the incoming radiation as coming from the left with amplitude A. The boundary conditions then attain the well-known form[19]

$$\mathcal{F}_+(0,t)=A(t)\ ,$$
$$\mathcal{F}_-(L,t)=0\ . \tag{9}$$

The second of these equations expresses the notion that there is no reflected wave at the back surface of the structure. The amplitude T of the transmitted wave now equals $\mathcal{F}_+(L,t)$, whereas the amplitude of the reflected wave R is equal to $\mathcal{F}_-(0,t)$. The solution of the nonlinear coupled-mode equations in conjunction with the boundary conditions appears to require numerical techniques.

The coupled-mode equations have important scaling properties that reduce the available phase space considerably. These become apparent when we make the substitutions $\delta=\alpha\tilde{\delta}$, $\kappa=\alpha\tilde{\kappa}$, $\Gamma=\beta^2\tilde{\Gamma}$, $\mathcal{F}_\pm=\sqrt{\alpha}\tilde{F}_\pm/\beta$, $z=\tilde{z}/\alpha$, $t=\tilde{t}/\alpha$, $A=\sqrt{\alpha}\tilde{A}/\beta$, and $L=\tilde{L}/\alpha$, where α and β are arbitrary numbers, and the coupled-mode equation and boundary conditions are seen to be unchanged. This means that we may fix Γ, as well as any one of the three parameters κ,δ,L without loss of generality. In the present work we choose $L=1$ and $\Gamma=0.1$ throughout. A

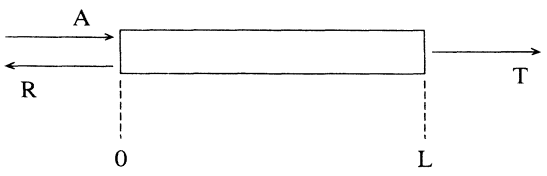

FIG. 2. Schematic of our geometry.

positive value for Γ implies a positive nonlinearity, and thus an increase of the index of refraction with field strength [Eq. (1)], causing the dispersion curves (Fig. 1) to shift down. The low-intensity limit can now thus be investigated by tuning close to the upper edge of the stop gap.

After these general comments regarding the coupled-mode equations we now briefly turn to the time-independent solutions. These solutions, which involve Jacobi elliptic functions, can be found by using, for example, the generalized Stokes parameters introduced by Daino, Gregori, and Wabnitz for the analysis of nonlinear directional couplers.[20] The results of such an exercise have previously been given explicitly by Winful, Marburger, and Garmire,[21] and will not be repeated here. We just point out that these solutions imply a bistable behavior for nonlinear periodic media with sufficient feedback. This is illustrated in Fig. 3. The lines in this figure give the transmissivity $|T|^2/A^2$ (Fig. 2) as a function of the incoming amplitude for a system with parameters $\kappa=5$ and $\delta=4.75$ (and $L=1$ and $\Gamma=0.1$). The frequency is thus chosen to be close to the upper edge of the stop gap (Fig. 1), so that we are in the low-intensity limit. Although a full time-dependent calculation is required to determine the stability of the various branches in the figure, an elementary analysis[22] shows that the dashed part is unstable against amplitude fluctuations. Such an analysis further shows that the solid parts are stable against such fluctuations, but our numerical work in Sec. III demonstrates that other instabilities render this picture incomplete.

On the lower stable branch the transmissivity is very low, and the system essentially behaves as if it were linear. As previously illustrated by Chen and Mills,[23] the energy density in this regime is indeed very similar to the negative exponential profile expected for linear systems. If the system is prepared so as to be on this lower branch, and the incoming amplitude is increased to about 1.60 (where the lower branch folds back), one would naively expect the system to jump from a low-transmission to a high-transmission state. The time-independent calculations of Chen and Mills[23] show that energy densities for states on this upper branch peak around the middle of the structure and are thus distinctly nonexponential. Similarly, if the system is initially on the upper branch, and the incoming amplitude is lowered below about 1.05, the system is expected to jump back to the lower branch. In Sec. III we demonstrate that this view is often too simplistic. Note that in following the upper branch, the system passes a point where the transmissivity equals unity. At this incoming amplitude (about 1.11 in Fig. 3) a gap soliton is excited. In Sec. III we study this simple picture in more detail by analyzing the results of numerical solutions to the coupled-mode equations.

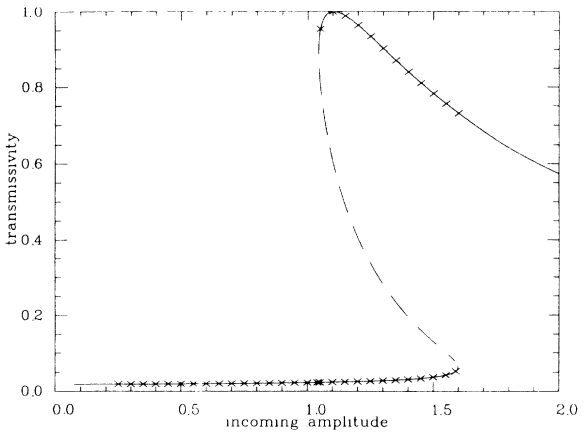

FIG. 3. Time-independent solutions of the coupled-mode equations for $\kappa=5.00$, $\delta=4.75$, $L=1$, and $\Gamma=0.1$. Solid lines: solutions stable to amplitude fluctuations. Dashed line: unstable solutions. The crosses ($\times$) indicate the results of time-dependent calculations. The size of the bistable region, which depends on the feedback provided by structure, grows with increasing L and κ, and with decreasing $|\delta|$.

III. NUMERICAL RESULTS

In this section we describe some of the numerical solutions to the coupled-mode equation [Eqs. (7)], with the restriction on the nonlinear coefficients as in Eq. (8), and boundary conditions given in Eqs. (9). Apart from the boundary conditions we of course need initial conditions as well. Throughout this work we use

$$\mathcal{F}_{\pm}(z,0)=0 , \tag{10}$$

so that the nonlinear structure initially contains no energy.

The detailed numerical procedure to integrate the resulting initial-value problem will be described in detail elsewhere, but can be roughly explained. The coupled-mode equations have the important property that the characteristics are straight lines. By the coordinate transformation

$$\begin{aligned} z&=\zeta-\tau , \\ \frac{c}{\eta}t&=\zeta+\tau , \end{aligned} \tag{11}$$

we can make the integration directions coincide with the characteristics. We then use standard finite-difference methods for solving ordinary differential equations to integrate the resulting equations. With the introduction of a finite-difference scheme, the characteristics form a two-dimensional regular grid. We now integrate each of the two equations over one of the set of characteristics, while combining the results at the grid points. The disadvantage of this method is that step sizes in the space and time directions cannot be chosen independently: A doubling, say, of the number of grid points inside the structure results in a doubling of the number of grid points in the time direction as well, thus quadrupling the total number of required integrations. In spite of this we have found the resulting procedure satisfactory for our purposes, typically using between 25 and 100 grid points inside the structure. The method is quite versatile and can

be used in other situations where a coupled-mode description can be used, for example, for the study of transverse instabilities in nonlinear slabs.[24] Moreover, the numerical method lends itself very well to vectorization.

In all our calculation we first let the system settle in a state on the lower branch (Fig. 3) with a certain value of the amplitude of the incoming radiation A. Such a dynamic equilibrium is characterized by a constant energy flux $|\mathcal{F}_+|^2-|\mathcal{F}_-|^2$ inside the structure. After the system settles we raise the incoming amplitude slightly (typically by 0.01, see Fig. 3), and again we let the system come to a dynamic equilibrium. We refer to this procedure as following the branch "adiabatically." In fact, the small increment is not even applied instantaneously, but rather is smeared out over a time interval equal to half the round-trip time of the system T_r, where

$$T_r=2\eta L/c \ . \tag{12}$$

As discussed at the end of Sec. II, for a certain value of the incoming amplitude the system will "jump" off the lower branch, which for a system with parameters as in Fig. 3 occurs where this branch folds back at $A\approx 1.60$. If the system then does settle at the higher branch, the incoming intensity is slowly decreased, so that the system adiabatically follows the upper branch back, until it jumps back to the lower branch ($A\approx 1.05$ in Fig. 3). A result of the described procedure is included in Fig. 3 represented by the crosses ($\times$). These indicate at which value of the transmissivity the system settles for a given incoming amplitude. For clarity, only one in five of the total number of calculated points have been shown in Fig. 3. In this situation the time-independent solutions are obviously a very good indicator of the full time-dependent behavior of the system. The time-independent solutions, however, give no indication as to how the system jumps, or how long it takes to settle. In order to answer these questions we refer to Fig. 4, which shows the transmitted amplitude while the systems jumps from the lower to the upper branch [Fig. 4(a)], and vice versa [Fig. 4(b)], for the system with the parameters as in Fig. 3. As the unit of time we take the round-trip time in the linear system T_r [Eq. (12)].

From Fig. 4(a) we see that it takes the system about 50 round-trip times to come to settle after jumping off the lower branch. This interval is seen to divide naturally into two parts, each lasting about 25 T_r. We denote these by "injection phase," and "oscillation phase," respectively. In the injection phase the system is essentially still in a (nonequilibrium) low-transmission state. This is illustrated by the dashed line in Fig. 5, which shows the energy density $|\mathcal{F}_+|^2+|\mathcal{F}_-|^2$ inside the structure after 15 T_r in Fig. 4(a). We see that although the energy distribution is definitely not a negative exponential (it peaks just behind the front surface), the decay near the back surface is qualitatively of this form. This field profile is typical for the injection phase, during which the energy density grows slowly, while the position of its maximum slowly moves backwards. The duration of the injection period depends on the details of the adiabatic following: Referring to Fig. 3, it varies with the amplitudes associated

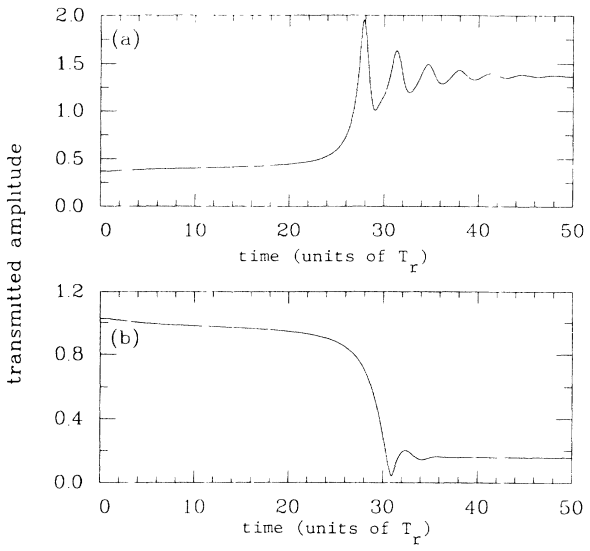

FIG. 4. (a) Time dependence of the transmitted amplitude $|T|$ (Fig. 2) during the transition from the low-transmission to the high-transmission state in Fig. 3 ($A=1.592$). The origin of time coincides with the application of the change in amplitude of the incoming radiation which leads the system to jump. (b) Same as (a), but for the transition from the high-transmission to the low-transmission state in Fig. 3 ($A=1.050$). The origin of time is defined similarly as above.

with the rightmost crosses on the lower and higher branches. If the latter is only just "over the edge" of the lower branch, the injection phase can take very long.

The oscillation phase in Fig. 4(a) is characterized by a damped oscillatory output at a level which is much higher than during the injection, while the state of the system finally settles on the higher branch in Fig. 3. Both

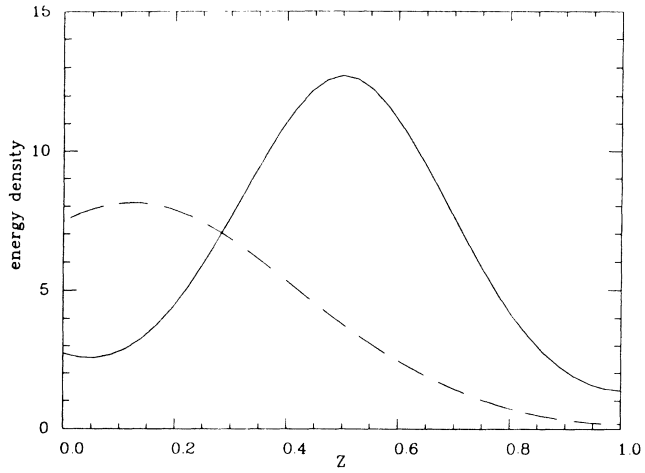

FIG. 5. Energy density inside the structure during transitions between branches. Dashed line: at $t=15\ T_r$ in Fig. 4(a). Solid line: at $t=30\ T_r$ in Fig. 4(a).

the period of the oscillation and its damping rate, which appear to be insensitive to the details of the adiabatic following, are caused by a "sloshing" of the energy inside the structure, of which the solid line in Fig. 5 gives a snapshot at $t=30\ T_r$. We consider this phenomenon in more detail in Sec. IV. However, it is clear that the field indicated by the solid line in Fig. 5 qualitatively differs from that in the injection phase (dashed line). It peaks roughly in the middle at a much higher value, and misses the near-exponential decay near the back surface. It should finally be mentioned that Fig. 5 is quite similar to energy profiles found from time-independent calculations, such as presented before by Chen and Mills.[23]

We conclude that during the injection phase the energy content of the structure increases sharply and that by the end the field profile has changed qualitatively. Since the frequency of the radiation lies within the stop gap of the linear structure, no traveling waves are allowed in most of the structure, resulting in an injection phase lasting tens of round-trip times. During the oscillation phase the system evidently properly distributes its newly gained energy. We have found that the described behavior is by no means general. Below we discuss situations in which the system never settles at all on the upper branch.

As mentioned, Fig. 4(b) shows the transmitted amplitude while the state of the system jumps from the upper branch back to the lower one. Again we see the equivalent of the injection phase, which lasts about 25 T_r, and an oscillatory phase which lasts only a few (about 5 T_r) round-trip times. It is our experience that this process *always* takes place in such a way. Because of this predictability of the jump down to the lower branch, we henceforth concentrate on the reverse transition.

We next show some results for two systems with the parameters $\delta=4.5$ and 4.0, while $\kappa=5.0$ in both cases (and, as always, $L=1$ and $\Gamma=0.1$). The time-independent solutions for these sets of parameters trace a curve very similar to that in Fig. 3, and are therefore not presented here. For both values of δ we follow the branch adiabatically until it folds back just as in Fig. 3. However, for neither value of δ does the system now settle on the higher branch. Although we cannot prove this statement rigorously, we have integrated the system with $\delta=4.5$ for well over 20 000 T_r without observing a tendency to relax. We illustrate this behavior again by showing the transmitted amplitude as a function of time. This amplitude can again be separated into an injection and an oscillation phase. The injection phase looks very similar to the one before (Fig. 5) and is not shown here. However, Fig. 6 shows the transmitted signals as they appear well into the oscillation phase, after possible transients have died out. The output is seen to be periodic in both cases, with a period of about 2.8 T_r for $\delta=4.5$ [Fig. 6(a)], and about 5.2 T_r for $\delta=4.0$ [Fig. 6(b)]. Apart from this, an important difference is that Fig. 6(b), in which we are tuned farther from the edge of the gap, appears much "spikier" than Fig. 6(a). As will be discussed in Sec. IV, this is a reflection of the mechanism that is ultimately responsible for these oscillations. A transmitted signal similar to Fig. 6(a) has been observed earlier by Winful and Cooperman[14] (for $\kappa=2.0$, $\delta=0.0$). However, these

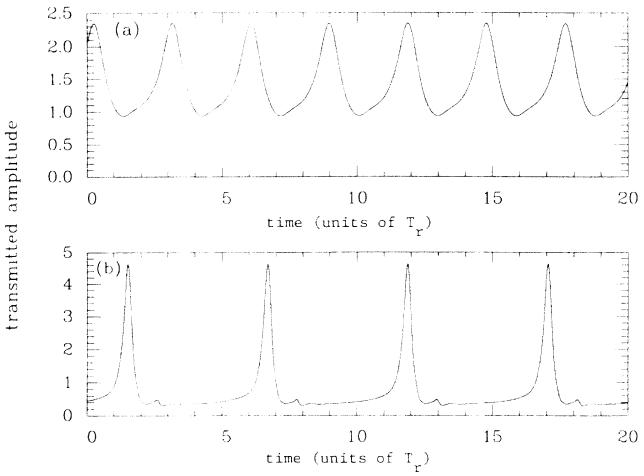

FIG. 6. (a) Transmitted amplitude $|T|$ well after jumping off the low-transmission branch for a system with parameters: $\kappa=5.0$, $\delta=4.5$, $L=1$, and $\Gamma=0.1$. The incoming has amplitude $A=1.97$ (Fig. 2). (b) Same as (a), but for system with parameters $\kappa=5.0$, $\delta=4.0$, $L=1$, and $\Gamma=0.1$. The incoming radiation has amplitude $A=2.625$.

authors apply their incoming amplitude instantaneously, thus creating large transients which may complicate the dynamics.

The transition between the regimes where the system eventually settles [as in Figs. 3 and 4(a)] and where it does not (as in Fig. 6) is estimated to be $\delta_t \approx 4.53$ for $\kappa=5.0$. For $\delta > \delta_t$ the system eventually settles; otherwise, it exhibits self-pulsations. The precise transition point is hard to determine since as $\delta \to \delta_t$, it takes an increasingly long integration time to determine the final state of the system. We have observed such a transition for several values of κ (see Sec. IV, especially Table I) and therefore believe it to be a general property of nonlinear periodic media. With increasing κL, the ratio δ_t/κ increases as well, so that increasing linear feedback moves the transition point closer to the stop-gap edge. We return to this matter in Sec. IV.

Comparing a series of different runs, as δ is decreased more and more at constant κ, the transmitted signal grows spikier, until, at $\delta \approx 3.5$, a period doubling appears to take place. The differences between the first and second halves of this new period are rather subtle and we therefore do not show the transmitted amplitude for this case. For $\delta \lesssim 3.5$ the nature of the transmitted amplitude turns much richer. Our calculations, which extend down to $\delta=0$ (the middle of the gap) with step sizes of 0.25, and then down to $\delta=-4.0$ with step sizes 1.0, show a wide variety of transmitted signals, which include simple periodic signals, period-n signals, where $n=2,5,6,7$ have been observed, as well as chaotic signals. However, no constant signals were observed for $\delta < \delta_t$. A systematic study of this complex behavior is rather difficult, as the observed signal appears to be very sensitive to the last stable position on the lower branch and the subsequent step size. For this reason we cannot give general rules regarding what kind of output to expect in a given situa-

tion. It should be mentioned that we have *not* observed the "classic" period-doubling route to chaos, but this may be due to the extreme sensitivity to the details of the choice of parameters. Further, the observed behavior is *not* due to our numerical procedure. If the integration steps are chosen to be small enough, the resulting transmitted signal is independent of the grid size.

As examples we now show the transmitted amplitudes well in the oscillation phase for $\delta=2.25$ [Fig. 7(a)] and $\delta=1.75$ [Fig. 7(b)], both with $\kappa=5.0$. We see that, compared to the signal in Fig. 6(b), for $\delta=2.25$ a period doubling has taken place, whereas for $\delta=1.75$ the transmitted amplitude does not seem to repeat itself at all. This is consistent with the power spectrum of the signal, which shows little structure except for two peaks at frequencies of $2\pi/T_a$ and $4\pi/T_a$, where T_a is the average "period" of the signal. Again, a transmitted signal similar to that in Fig. 7(b) has previously been observed by Winful and Cooperman,[14] but only after an instantaneously switched on incoming signal. In Sec. IV we analyze the results presented thus far. We now close the present section with the characterization of the chaotic signal of Fig. 7(b).

As mentioned in Sec. II, the coefficients in the coupled-mode equations are taken to be real so that local energy dissipation is not allowed. In fact, it has been shown[6] that under this restriction the coupled-mode equations can be derived from a Hamiltonian function. However, the reflected and transmitted energy introduce losses on a global scale, so that, in effect, the global dynamics is not Hamiltonian in nature, but is dissipative. While not explicitly mentioned, the transmitted amplitudes in Figs. 6 and 7(a) can of course be associated with a fixed-point and limit-cycle attractors, respectively. Similarly, since the global dynamics of the system is dissipative, and the transmitted amplitude in Fig. 7(b) is chaotic, it must be associated with a strange attractor.[25] We obtained the clearest view of this attractor by plotting the imaginary part of the transmitted signal versus the real part, with time as the parameter. This results in the *D*-shaped object shown in Fig. 8, with the loop of the *D* corresponding to the spikes in Fig. 7(b). Actually, Fig. 8 shows the calculated points, which are separated by $T_r/128$, connected by straight lines to aid the eye.

We now turn to the dependence on the initial conditions of the trajectories on the attractor. To do so we compare two runs which we start well in the oscillation phase with initial conditions differing by 10^{-13} at a single grid point. The transmitted intensities in these two runs diverge exponentially fast until, at $t\approx 150\ T_r$, the difference is of the order of magnitude of the signal itself, and saturation sets in. We thus see an extreme dependence on initial conditions, indicating that the strange attractor is characterized by a positive (largest) Lyapunov exponent,[25] which we estimate to be about $0.2/T_r$.

Another way to characterize a strange attractor is by its fractal dimension.[26] A commonly used procedure is due to Grassberger and Procaccia[27] and is based on the correlation integral of points on the attractor. This method leads to the so-called correlation exponent. However, this method fails to converge for our attractor. We believe this is due to its shape: With the large empty region in the middle, it is understandable that distant parts of the attractor appear to have the dimension of a simple line. We therefore think that the correlation integral is sensitive to both this appearance as well as to the intrinsic dimension of the attractor, resulting in the failure of the method. Instead we have used a method proposed by Badii and Politi,[28] which is based on nearest-neighbor distances of points on the attractor. This method leads to the so-called information dimension

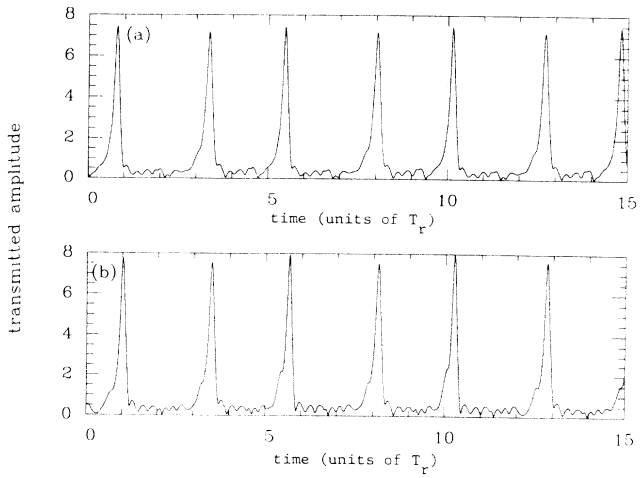

FIG. 7. (a) Same as Fig. 6. The parameters are $\kappa=5.0$, $\delta=2.25$, $L=1$, and $\Gamma=0.1$. The incoming amplitude $A=4.29$. (b) Same as Fig. 6. The parameters are $\kappa=5.0$, $\delta=1.75$, $L=1$, and $\Gamma=0.1$. The incoming amplitude is $A=4.66$.

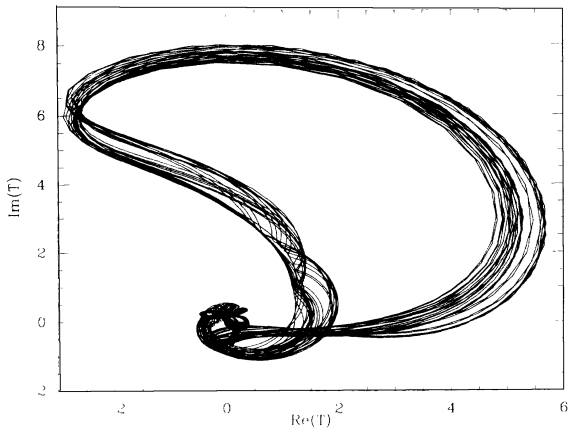

FIG. 8. Real part of the transmitted amplitude (horizontal axis) vs imaginary part (vertical axis) with time as parameter for the chaotic signal in Fig. 7(b). The actual data points, which are intervals of $T_r/128$ apart, are connected by straight lines to aid the eye.

D_I of the attractor,[29] which is a lower bound to the Hausdorff dimension. Following the procedure recently described by Broggi,[30] we find that $D_I = 2.3 \pm 0.05$. Details of this calculation can be found in the Appendix. Since the dimension of a set corresponds roughly to the amount of information needed to accurately specify points in it, we can interpret our finding as an indication that for the description of the chaotic signal in Fig. 7(b) only a few parameters are relevant.[25] Alternatively, one should be able to describe the dynamics by only a few coupled equations.

IV. DISCUSSION AND CONCLUSIONS

In this section we give a qualitative explanation of the behavior observed in Sec. III. In particular we would like to understand why, after jumping off the lower branch, the system eventually settles when we tune close enough to the edge of the stop gap [Figs. 3 and 4(a)], while otherwise it remains in a self-oscillating state (Figs. 6 and 7). We have not yet been able to devise a quantitative theory, but we think we have identified the probable causes of the instability. As a preliminary step let us consider the field profiles in Fig. 5 again. The dashed line in this figure shows a typical low-transmitting state (albeit a nonequilibrium one). The energy flow is of course small because the energy density is generally too low to tune the radiation out of the gap and, consequently, any possible transmitted radiation has to tunnel through a large fraction of the structure. It is especially the near-exponential tail at the back of the structure that limits the tunneling rate. The solid line in Fig. 5 shows a typical (nonequilibrium) high-transmitting state. The energy density in the middle section is now high enough to allow traveling waves. Transmitted radiation thus has to tunnel only through two thin regions at the edges only, thus allowing a substantial energy flux. However, another scenario seems just as likely: Once the light has tunneled from the left into the middle section it is surrounded by two high-reflectivity regions. The situation then is very similar to that of light trapped in a Fabry-Pérot interferometer, except that here the interferometer ensues from the dynamical interaction of the light and the medium. This "transparent region" can thus travel through the structure, creating a second way in which energy can be transported.

We can quantify the intuitive notion developed above by estimating the required energy to create locally a transparent region. To do so we borrow some of the results of our earlier work on gap solitons, which makes use of the Bloch function at the edges of the stop gap of the linear structure. Using our present notation, the envelope functions multiplying these Bloch functions are found to be proportional to $\mathcal{F}_+ \pm \mathcal{F}_-$. Rewriting our previous results[2] in this way shows that when

$$\frac{3\Gamma}{8(\kappa-\delta)}|\mathcal{F}_+ - \mathcal{F}_-|^2 > 1 \ , \tag{13}$$

the field is sufficient to tune the system locally out of the gap. Some remarks concerning this result should be made: Eq. (13) only holds if the nonlinearity is positive, and is strictly speaking only valid in the low-intensity limit.[2] Further, it is based on a time-independent analysis and thus does not take the dynamics of the transparent region into account. We have developed a more general criterion which does include propagation effects,[4] but in light of our restriction to low intensity, and because we only require a rough idea of the extent of the transparent region, we have found the criterion in Eq. (13) sufficient for our purposes. We now first apply this criterion to indicate where the radiation has tuned itself out of the stop gap for $\kappa = 5.0$ and $\delta = 4.75$ (Fig. 9). This allows for a direct comparison with Figs. 3–5 and with the discussion in the first paragraph of this section. The shaded region in Fig. 9 indicates the transparent region, whereas the remainder only allows energy transport through tunneling. Notice that the front of the structure in this figure appears at the bottom. The figure indeed shows the transparent region moving from the front of the structure to the middle. This movement, as well as the subsequent relaxation oscillations, are well correlated with the transmitted amplitude shown in Fig. 4(a). Notice also the small transparent region forming at about 28 T_r at the front of the structure. It is created while the edge of the large transparent region is farthest removed from the front of the structure (by about 0.4). Presumably the tunneling rate has dropped so much at this point that the energy is trapped and cannot enter the larger transparent region at a sufficient rate. However, about a single round-trip time later the edge is much closer by and the resulting increase in the tunneling rate allows the energy to flow to the transparent region in the middle of the structure.

We next investigate in a similar way a situation in which the system exhibits self-oscillations. We now take $\kappa = 5.0$ and $\delta = 4.0$ so that, according to Fig. 6(b), the transmitted signal is periodic. The result, which is shown in Fig. 10, has the same time origin as Fig. 6(b). Figure 10 differs quite dramatically from Fig. 9 since the large

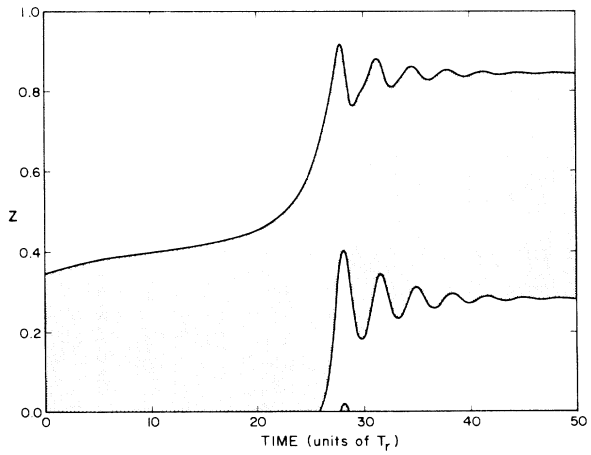

FIG. 9. Position of the transparent region (shaded) as a function of time. The parameters and the origin of time are the same as in Fig. 3.

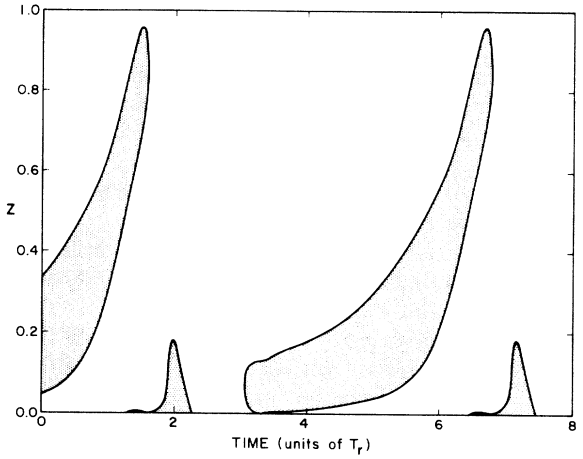

FIG. 10. Position of the transparent region (shaded) as a function of time. The parameters and the origin of time are the same as in Fig. 6(b).

transparent region in the middle does not exist at all times. A comparison with Fig. 6(b) shows that the spikes in the transmission occur when the transparent region is closest to the back surface of the structure. This region ceases to exist almost immediately after that, implying that the spikes in the transmitted signal carry a large fraction of the energy content of the transparent region. A smaller fraction of this energy is reflected back into the structure. The dynamics of this large transparent region is clarified by a study of the energy density in the structure. This quantity is shown in Fig. 11 for $t=T_r$ and $t=1.25\ T_r$. These profiles remind one of a soliton propagating to the right through the structure. However, upon collision with the back surface the soliton is destroyed, and, as discussed, most of its energy leaves the structure.

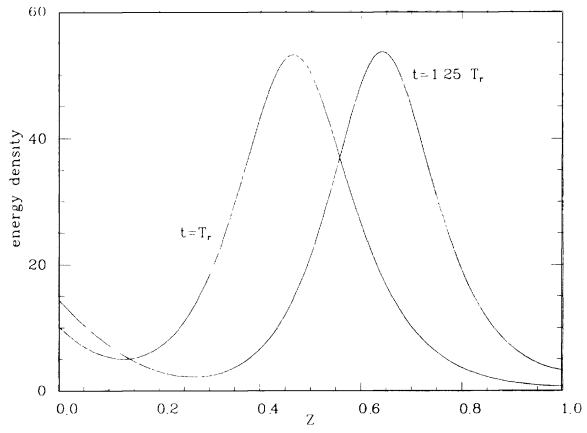

FIG. 11. Energy density at $t=T_r$ and 1.25 T_r in Fig. 13 while the structure self-oscillates. Note that the shape hardly changes in this time interval, suggesting that these field profiles are associated with a soliton or solitary wave of the system.

We believe that the formation and subsequent destruction of a large transparent region (soliton) dominates the dynamics inside the structure in the interval between $t\approx 3$ T_r and 6.5 T_r in Fig. 10. More puzzling is the creation and particularly the disappearance of the small pocket of transparency at the front surface around $t=2\ T_r$ (cf. Fig. 9 and the discussion in the preceding paragraph). Just as in Fig. 9, it appears when the large transparent region is about $z=0.4$ away, again, presumably because the tunneling rate to the rest of the structure has dropped too much. However, as opposed to the situation above, it now vanishes well before the next transparent region is created. A study of the reflected amplitude, in conjunction with that of the time-dependent energy density inside the structure (which are not shown here) reveals that the small transparent pocket vanishes after interaction with the reflected waves from the collision of the soliton with the back surface, about $T_r/2$ earlier. Thus although a large fraction of the energy in the large transparent region leaves the system, a smaller fraction is reflected to the front of the structure. After a time delay, therefore, this energy returns to the front surface, influencing (in this case, hindering) the buildup of a new transparent region.

As mentioned, while the large transparent region moves to the back (Fig. 11), the energy density inside the structure reminds one very much of a traveling soliton or solitary wave. Since it is known that the coupled-mode equations have stable solitary-wave solutions on an infinite interval,[6] we conjecture that the energy is indeed transported to the back of the structure by such a solitary wave, hence the nomenclature already used above. Of course, the solitary wave is destroyed upon interaction with the rear surface. If one identifies energy transport through tunneling as a kind of conduction process, one can think of the solitonic energy transport as a kind of convection. We mention in passing that our previous work[2] has shown that when the field is tuned close enough to the edge of the stop gap, the solitary wave is in fact a soliton of the nonlinear Schrödinger equation.

We are now ready to discuss a few of the general observations we made in Sec. III. The first of these is the tendency of the transmitted signal to get spikier when the radiation is tuned farther away from the edge of the stop gap. We think that the width of the transmitted pulses is a reflection of the width of the solitary wave which carries the energy through the structure. Previous work of ourselves[2] and others[6] have shown that these solitary waves get sharper when the field is tuned farther away from the edge of the stop gap. If dynamic effects are ignored (i.e., when the solitary wave is at rest), and we are tuned close to the stop-gap edge, the width W of the solitary wave is given by[2]

$$W=\frac{1}{\sqrt{2\kappa(\kappa-\delta)}}\ . \tag{14}$$

Given its restricted validity, as well as the uncertainty regarding the interaction of the solitary wave and the back surface, this expression should not be taken too seriously. Still it predicts the right trend and we believe that it does contain the essential physics.

Our observations lead immediately to two more conclusions. The first of these is that because of the convective energy transport from the front to the back of the structure, and the back reflection of a small portion of this energy, the parameters of the self-oscillation, like the period, are hard to predict. For example, the interaction of the reflected energy with the buildup of a new transparent region at the front surface is a rather subtle effect, and an estimation of the various time intervals involved requires a thorough understanding of the dynamics. The second conclusion we can draw refers to the onset of chaotic oscillations, which occurs if we are tuned sufficiently far from the stop-gap edge. This onset of instability reminds one of that first described by Ikeda, Daido, and Akimoto[31] for a ring cavity. The similarity is actually quite close since the role of a delay time, which is crucial in their argument, is here played by the time interval required for the reflected fraction of the convectively transported energy to return to the front surface. Unfortunately we have no direct control over this time interval, so that comparison with the predictions of the model in Ref. 31 cannot be made. However, for a fixed delay time that model leads to chaotic behavior[22,31] when the intensity is raised sufficiently. This agrees very well with our observations in Sec. III.

The last matter to be discussed is the transition from a constant to a periodic transmitted amplitude, which, for $\kappa=5.0$ takes place at $\delta_t \approx 4.53$. We saw earlier that at this point the conductive type of energy transport is replaced by a convective type. Presumably the former is more efficient close to the edge of the stop gap, whereas the latter takes over when deeper inside. It is intuitively clear why such a transition should exist: If the soliton is about as wide as the total structure the energy can propagate freely throughout. As a consequence energy hardly has to tunnel (if at all) in order to reach the back side. Close to the edge of the gap, therefore, this is the most efficient type of energy transport. From Eq. (14) we see that the soliton gets narrower when we are tuned deeper into the gap. Consequently, the transparent region gets narrower as well, and therefore the tunneling rate drops, decreasing the efficiency of the conductive type of energy transport. This can be expected to be quite a dramatic effect as the tunneling rate is an exponential function of the parameters. The efficiency of the convective type of energy transport depends in a far less critical way on the position in the gap. One may argue that at most it depends linearly on the soliton width, but certainly not exponentially. It is thus to be expected that when we tune deeper into the gap and the soliton narrows, the convective type of energy transport must eventually be more efficient. Of course this necessitates a δ_t where the two processes are equally efficient. Quantifying this argument is again hard because the soliton width is a dynamic variable. To lowest order, however, one might argue that the transition occurs at a fixed ratio μ of the static soliton width W [Eq. (14)], and the system's length L. This assumption immediately leads to an expression for the onset of self-oscillation:

$$\frac{\delta_t}{\kappa}=1-\frac{1}{2(\mu\kappa L)^2} . \tag{15}$$

This simple expression exhibits the proper trend: For increasing κ the onset of self-oscillation occurs closer and closer to the edge of the stop gap. Equation (15) can be tested qualitatively by using known values of δ_t at various values for κ and solving for μ to see if it is indeed a constant. The results of such an exercise are given in Table I. This table shows that μ is *not* constant, but varies slightly with κ, and has a value of about 0.50. Still, in spite of the various approximations leading to Eq. (15) there is good qualitative agreement between the predictions of this equation and our numerical results: μ does not vary by much and, in addition, its value of about 0.50 not only agrees very well with Fig. 9, but also with our expectations. Based upon the argument earlier in this paragraph, on the one hand one expects the soliton to fit well in the structure, while on the other hand it should not be too narrow because of the resulting low tunneling probability. The fact that our simple argument, which was only based upon the expectation that μ be constant, leads to a value which agrees well with our intuition makes us believe that the discussion leading to Eq. (15) is based upon the correct physical arguments.

As a final remark we mention that Coste and Peyraud,[9] in their investigations, observe behavior that is similar to that described here. Using the δ-function model mentioned in the Introduction, they consider a semi-infinite medium with energy coming from one side and find the following behavior: Below a certain value of the incoming intensity the field settles into a low-transmission state, in qualitative agreement with our observations. However, above this threshold they find that solitary waves are intermittently generated at the front surface, whereupon these waves travel inside the structure. Although this behavior is reminiscent of Fig. 7(b), there are some considerable differences: they do not observe their semi-infinite system settling on the high-transmission branch as in Fig. 3, or the periodic behavior as in Fig. 6. The observation of the intermittently generated solitary waves in a semi-infinite system seems to contradict our discussion earlier in this section where we concluded that the chaotic behavior was related to the back-reflected energy initially carried by the solitary waves. We should, however, keep in mind that Coste and Peyraud's model is known to introduce artifacts (see the discussion in Sec. I) and it is not clear whether their observed behavior belongs to this category too. Moreover, it is curious that they have not observed their system to settle on the high-transmission

TABLE I. The onset of self-oscillation δ_t as following from our numerical work, for various values of κ. We can use these in Eq. (15) to solve for μ, which is the ratio of the soliton width and the system's length.

κ	δ_t	μ
4.0	3.48±0.01	0.490±0.005
5.0	4.53±0.01	0.461±0.005
6.0	5.59±0.01	0.451±0.006
7.0	6.67±0.01	0.480±0.008
8.0	7.77±0.01	0.510±0.011
9.0	8.80±0.01	0.541±0.015

branch for any choice of parameters. One would expect any reasonable model to exhibit such behavior in some appropriate part of phase space. Finally, it should be pointed out that a model in which the dielectric is concentrated in δ-function-like planes is very much unlike ours since inequality (2) is not satisfied. To the contrary, in fact, $n_0 \ll n_1$. The contradicting conclusions of Coste and Peyraud on the one hand, and ours on the other, may thus well be due to the rather significant differences in the models.

In conclusion, we have numerically investigated the time-dependent properties of nonlinear periodic media. The driving fields were adjusted adiabatically so that a meaningful comparison with the well-known time-independent solutions of the coupled-mode equations is possible. We find very rich dynamics, exhibiting gap solitons, as well as periodic and chaotic self-oscillation. These two regimes are characterized by a different type of energy transport through the structure: In the gap soliton regime energy is transported by a tunneling process, whereas the oscillatory regime is characterized by a convective type of transport, in which the energy is carried by solitary waves. We further believe that these periodic oscillations turn chaotic when a sufficient amount of the energy carried by the solitons is back-reflected towards the front of the structure, where it interferes with the formation of the next soliton. This process is similar to the instability described by Ikeda, Daido, and Akimoto in ring lasers. We are currently working on a more quantitative description, and we expect to report on this work in a future publication.

ACKNOWLEDGMENTS

We thank K. R. Jackson for help with some of the numerical aspects of this work, and N. B. Abraham for bringing our attention to Ref. 30, as well as for a useful discussion with one of us (J.E.S.). This research was supported by the Ontario Laser and Lightwave Research Centre.

APPENDIX

In this appendix we describe briefly our procedure to obtain the information dimension D_I of the attractor in Fig. 8. As mentioned in Sec. III, our method makes use of the nearest-neighbor distance distribution of points on the attractor. While this class of methods was proposed by Badii and Politi,[28] in the implementation we follow recent work by Broggi.[30]

The method calls for two independent scalar time series consisting of equidistant samples of the chaotic signal $x_i \equiv x(t_0+(i-1)\tau)$ and $y_j \equiv y(t_1+(j-1)\tau)$. Recall from Sec. II that independence of the time series can be assured by starting with different initial conditions and integrating over about 150 T_r. Each of these time series is used to construct a representation of the attractor in an E-dimensional embedding space by introducing the vectors

$$\mathbf{x}(t)=\{x(t),x(t+\tau),\ldots,x(t+(E-1)\tau\} , \qquad \text{(A1)}$$

and similarly for y. However, to ensure the lasting independence of $\mathbf{x}$ and $\mathbf{y}$ we define the "data points" $\mathbf{x}_i \equiv \mathbf{x}(t_0+(i-1)\tau)$, where $i=1,2,\ldots,N$, whereas for the "reference points" $\mathbf{y}_j \equiv \mathbf{y}(t_1+(j-1)E\tau)$, where $j=1,2,\ldots,m$. These definitions ensure that all but the last $E-1$ samples x_i are elements in exactly E vectors $\mathbf{x}$, whereas each sample y_j is used as element in a single vector $\mathbf{y}$ only. Following Broggi[30] we now define $\Delta_{j,k,E}(n)$ as the Euclidean norm, computed in the E-dimensional embedding space, between a reference point $\mathbf{y}_j$ and its kth nearest neighbor chosen among n data points $\mathbf{x}$. Making use of these quantities, Badii and Politi[28] have shown that D_I can be estimated from the asymptotic relation

$$D_I \sim -\frac{\log_b(n/k)}{\frac{1}{m}\sum_{j=1}^{m}\log_b \Delta_{j,k,E}(n)}, \quad n\to\infty \qquad \text{(A2)}$$

where any base b for the logarithm may be used. Following Broggi again, we take $b=2^{0.25}$ so that a factor of 2 corresponds to four units.

The onset of the scaling regime in which Eq. (17) is valid was shown by Broggi[30] to depend critically on the selected value of k. This author comes to the conclusion that onset of scaling can be shifted to lower n by taking k small enough. However, doing so results in more noise, leading to a large uncertainty in estimating D_I. For a given number N of data points $\mathbf{x}$, therefore, one must choose k to be the largest value for which the onset of scaling can clearly be established.

In our implementation of this procedure we take $\tau=T_r/4$, $E=8$, while $m=1700$ and $N=191\,360$. We show in Fig. 12 the running estimate for D_I as a function

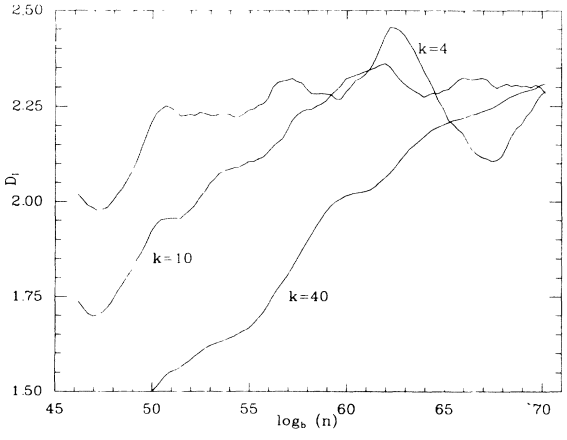

FIG. 12. Running estimate of the information dimension D_I as a function of the number of used data points n. Scaling is seen to set in at $\log_b n \approx 65$. The constant b equals $2^{0.25}$, so that an octave corresponds to four units. Based on this figure D_I is estimated to be about 2.3.

of n, where $N/64 \leq n \leq N$, and $k=4$, 10, and 40. The choice $k=4$ leads to a strongly fluctuating result, whereas for $k=40$ scaling has not yet set in, in agreement with the discussion of Broggi.[30] The value $k=10$ has been chosen such that the onset of the scaling regime is easily recognized to be around $\log_b n \approx 65$ ($n \approx 80\,000$). From Fig. 12 we conclude that $D_I = 2.30 \pm 0.05$, as stated in Sec. III.

[1]W. Chen and D. L. Mills, Phys. Rev. Lett. **58**, 160 (1987).
[2]C. M. de Sterke and J. E. Sipe, Phys. Rev. A **38**, 5149 (1989).
[3]U. Trutschel and F. Lederer, J. Opt. Soc. Am. B **5**, 2530 (1988).
[4]C. M. de Sterke and J. E. Sipe, Opt. Lett. **14**, 871 (1989).
[5]S. Wabnitz, Opt. Lett. **14**, 1071 (1989).
[6]A. B. Aceves and S. Wabnitz, Phys. Lett. A **141**, 37 (1989).
[7]J. Peyraud and J. Coste, Phys. Rev. B **40**, 12201 (1989).
[8]S. Dutta Gupta, J. Opt. Soc. Am. B **6**, 1927 (1989).
[9]J. Coste and J. Peyraud, Phys. Rev. B **39**, 13086 (1989).
[10]C. M. de Sterke and J. E. Sipe, Phys. Rev. A **39**, 5163 (1989).
[11]D. L. Mills and S. E. Trullinger, Phys. Rev. B **36**, 947 (1987).
[12]D. N. Christodoulides and R. I. Joseph, Phys. Rev. Lett. **62**, 1746 (1989).
[13]D. J. Kaup and A. Newell, Lett. Nuovo Cimento **20**, 325 (1977).
[14]H. G. Winful and G. D. Cooperman, Appl. Phys. Lett. **40**, 298 (1982).
[15]H. Kogelnik, Bell. Syst. Tech. J. **48**, 2909 (1969).
[16]H. Kogelnik, in *Integrated Optics*, edited by T. Tamir (Springer, Berlin, 1979), p. 15.
[17]G. P. Agrawal, *Nonlinear Fiber Optics* (Academic, San Diego, 1989), Chap. 7.
[18]C. M. de Sterke and J. E. Sipe, J. Opt. Soc. Am. A **7**, 636 (1990).
[19]H. Kogelnik and C. V. Shank, J. Appl. Phys. **43**, 2327 (1972).
[20]B. Daino, G. Gregori, and S. Wabnitz, J. Appl. Phys. **58**, 4512 (1985).
[21]H. G. Winful, J. H. Marburger, and E. Garmire, Appl. Phys. Lett. **35**, 379 (1979).
[22]H. M. Gibbs, *Optical Bistability: Controlling Light with Light* (Academic, Orlando, 1985).
[23]W. Chen and D. L. Mills, Phys. Rev. B **36**, 6269 (1987).
[24]B. D. Robert and J. E. Sipe (unpublished).
[25]D. Ruelle, *Chaotic Evolution and Strange Attractors* (Cambridge University Press, Cambridge, 1989), p. 20.
[26]B. Mandelbrot, *The Fractal Geometry of Nature* (Freeman, New York, 1983).
[27]P. Grassberger and I. Procaccia, Physica D **9**, 189 (1983).
[28]R. Badii and A. Politi, J. Stat. Phys. **40**, 725 (1985).
[29]J. D. Farmer, Z. Naturforsch. **37a**, 1304 (1982).
[30]G. Broggi, J. Opt. Soc. Am. B **5**, 1020 (1988).
[31]K. Ikeda, H. Daido and O. Akimoto, Phys. Rev. Lett. **45**, 709 (1980).

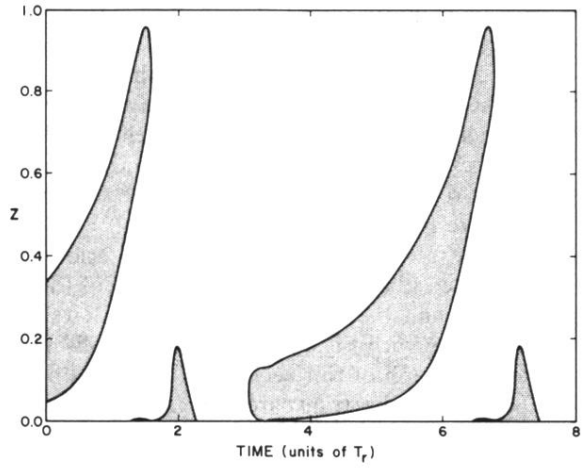

FIG. 10. Position of the transparent region (shaded) as a function of time. The parameters and the origin of time are the same as in Fig. 6(b).

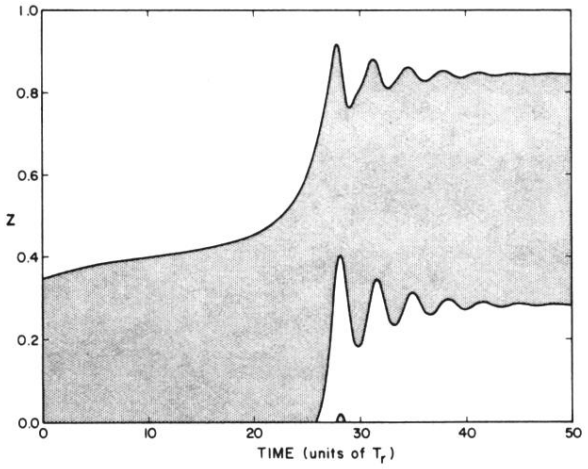

FIG. 9. Position of the transparent region (shaded) as a function of time. The parameters and the origin of time are the same as in Fig. 3.